Experimental characterization of fast electron stopping power in dense media ranging from solid to warm and dense matter

J.J. Santos[1], S. Hulin[1], B. Vauzour[1], X. Vaisseau[1], D. Batani[1], R. Bouilleaud[1], F. Deneuville[1], F. Dorchies[1], J.-L. Feugeas[1], C. Fourment[1], E. d'Humières[1], Ph. Nicolai[1], V.T. Tikhonchuk[1], M. Touati[1], A. Debayle[2], J.J. Honrubia[2], L. Gremillet[3], T. Ceccotti[4], V. Floquet[4], R. Benocci[5], A. Morace[5], M. Veltcheva[5], L. Volpe[5], S.D. Baton[6], F. Pérez[6], H.-P. Schlenvoigt[6], V. Yahia[6], F.N. Beg[7], S. Chawla[7], L.C. Jarrot[7], J. Peebles[7], H. Sawada[7], A. Sorokovikova[7], M. Wei[8], R. Fedosejevs[9], S. Kerr[9], M. Coury[10], R. Gray[10], P. McKenna[10], K. Li[11], J.R. Davies[12], Y. Rhee[13], H. McLean[14], P. Patel[14]

[1] *Université de Bordeaux-CNRS-CEA, CELIA, UMR 5107, Talence, France*

[2] *ETSI Aeronáuticos, Universidad Politécnica de Madrid, Spain*

[3] *CEA-DAM-DIF, F-91297 Arpajon, France*

[4] *CEA-IRAMIS-SPAM, Gif-sur-Yvette, France*

[5] *Dipartimento di Fisica, Universitá di Milano-Bicocca, Milan, Italy*

[6] *LULI, Ecole Polytechnique, CNRS/CEA/UPMC, UMR 7605, Palaiseau, France*

[7] *University of California, San Diego, La Jolla, USA*

[8] *General Atomics, San Diego, USA*

[9] *University of Alberta, Canada*

[10] *SUPA, University of Strathclyde, Glasgow, UK*

[11] *GoLP, Instituto de Plasmas e Fusão Nuclear - Laboratório Associado, Instituto Superior Técnico, Lisboa, Portugal*

[12] *Laboratory for Laser Energetics, University of Rochester, USA*

[13] *Korea Atomic Energy Research Institute, Republic of Korea*

[14] *Lawrence Livermore National Laboratory, Livermore, USA*

The predicted high gain of the fast ignition scheme (FI) for inertial confinement fusion makes it a candidate for industrial energy production [1]. This scheme demands a high-intensity laser system, $\approx 10^{20}\,\mathrm{W/cm^2}$, delivering an energy of $\sim 100\,\mathrm{kJ}$, generating a high current ($>\mathrm{GA}$) fast electron beam (FEB) with a mean kinetic energy in the range of 1-2 MeV. This beam must deposit a minimum of $\sim 20\,\mathrm{kJ}$ over 20 ps into a $20\,\mu\mathrm{m}$ radius hot spot in the compressed fuel [2]. This requires a high laser-to-FEB energy transfer, with weak angular dispersion. The subsequent FEB transport through the steeply increasing density and temperature profiles of the DT plasma determines the efficiency of the energy coupling to the hot spot. This paper is concerned with the FEB energy loss mechanisms in warm dense matter, which, in particular, remain poorly known

close to the FEB source. The main question is whether the resistive processes driven by the extreme current densities at play ($\sim 10^{14}$ A/cm^2) may enhance significantly the FEB dissipation far from the core, and, if so, whether this could compromise, or help, ignition.

The experiments presented here, carried out using sub-ignition energy laser facilities, aimed at benchmarking the widely used hybrid model for FEB transport in dense media ranging from solid to warm dense matter [3, 4, 5]. This approach assumes that the FEB is efficiently neutralized by a return current made of thermal electrons ($\vec{j}_h \approx -\vec{j}_e$), which implies a background plasma much denser than the FEB. The two electron populations can then be treated differently: the weakly collisional FEB is modeled kinetically whereas the highly collisional return current is described as an inertialess fluid. The FEB transport is then subjected to both binary collisions with the target bound and free electron, and the resistive electric field $\vec{E} = \eta \vec{j}_e$, where η is the background electrical resistivity. The components of the stopping power related to these mechanisms are, respectively, proportional to the background target density, $\frac{dW}{dz}|_{coll} \propto \rho$, and to the amplitude of the FEB current density, $\frac{dW}{dz}|_{res} \approx e\eta j_h$.

The first experiment was performed at the CEA-Saclay UHI100 facility. The goal was to study FEB transport using high-contrast ($> 10^{10}$) laser pulses interacting with well-characterized metallic foils. The laser pulse delivered 0.7 J on multi-layered Al/Cu/Al targets, with 25 fs duration and 800 nm wavelength. The resulting on-target intensity was $> 10^{19}$ W/cm^2. The use of a double plasma mirror ensured a steep density gradient at the time of the laser peak.

The temperature reached at the target rear surface was measured for varying thicknesses by collecting the thermal optical emission with a time-resolved narrowband ($\lambda = 532 \pm 10$ nm) imaging system [green symbols in Fig. 1-a)]. The measurements are fairly reproduced by a 3-D hybrid simulation [6] using as input the FEB distribution predicted by a 2-D PIC simulation of the laser-plasma interaction (dashed line). The latter indicates a 10% laser-to-FEB conversion efficiency. For a 20 μm-thick target, the temperature drops from > 100 eV at the front side to ~ 20 eV at the rear side.

An improved version of a semi-analytical model [7] was also successfully confronted to the experimental data and hybrid simulation results (solid lines). This model assumes that the FEB radial spread increases linearly with depth. Its short computation time (one second *vs* one day for the hybrid code) allows parametric studies of the FEB transport, regarding, in particular, the influence of the FEB initial spot size ($\Phi_0 \approx 15\,\mu$m) and angular divergence ($\theta \approx 10°$). Figure 1-b) plots the drag (green symbols) and resistive (orange symbols) contributions to the target heating: the resistive effects are seen to prevail up to 6 μm where the electrostatic field is $> 10^{10}$ V/m. The resistivity subsequently weakens, and so does the electrostatic field, because of

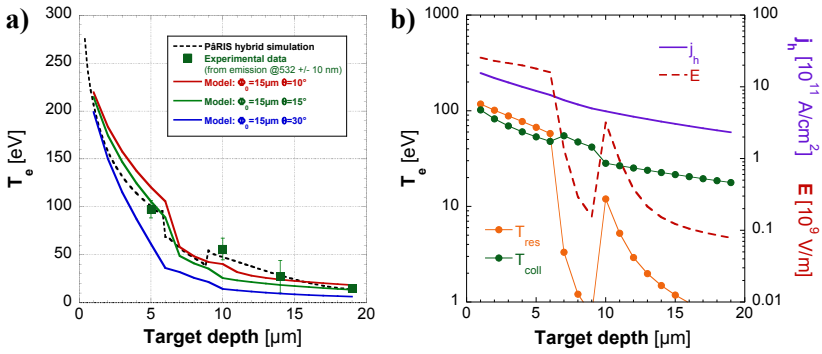

Figure 1: **a)** Background electron temperature against target depth. **b)** Longitudinal electric field (red dashed line), relativistic electron current (purple solid line), background electron temperature due to resistive heating (orange circle symbols) and due to electron/electron collisions (green circle symbols) against target depth.

the embedded $3\,\mu$m Cu layer. At larger depths, the FEB current density dramatically drops from 10^{12} at $z=0$ down to $5\cdot10^{11}$ A/cm^2 at $z=10\,\mu$m, hence making the drag stopping predominant.

The FEB transport was also studied in warm and dense matter. To this goal, Al foils were shock-compressed to a few times the solid density by a $2\omega_0$, ns pulse with a flat-top focal spot. The FEB was generated by a high-intensity, $1\omega_0$ short pulse in two different configurations: 35 J, 1 ps at LULI2000 and 135 J, 0.7 ps at TITAN-JLF, yielding on-target intensities of 10^{19} W/cm^2 and 10^{20} W/cm^2, respectively. The FEB was injected counter-current to the shock, through a plasma homogeneous in the transverse direction to first approximation. We used multi-layer foil targets with an Al propagation layer of variable thickness (hereunder called sample) and three fluorescent tracer layers of different atomic number to diagnose the FEB transport. These were embedded on both the front side, ($5\,\mu$m Ag) to quantify the FEB source, and on the rear side ($10\,\mu$m Sn plus $10\,\mu$m Cu) to quantify the electron flux through the sample. Figure 2-b) shows that the fluorescence ratio, Sn-K$_\alpha$/Ag-K$_\alpha$, decreases with the areal density of the sample with no clear difference between the solid or compressed cases. Given the 1D compression geometry, this is indicative of negligible resistive effects.

The sample-integrated energy losses predicted by hybrid simulations [5] are plotted in Fig. 2-a) as a function of the thickness of the sample and for three different laser energies (35, 70 and 350 J, hence yielding increasing FEB current densities). A fixed 40% laser-to-FEB conversion efficiency is assumed. In all cases, the simulated collisional losses prevail in compressed samples, and prove mostly unchanged for solid or compressed samples of equal areal density.

The lower-current results (parameters of the LULI2000 experiment, giving a mean current density of $8\cdot10^{10}$ A/cm^2 at the Ag interface with the Al-sample) demonstrate enhanced resistive losses in compressed samples. This can be attributed to the increased resistivity due to the shock-induced heating to the Fermi-temperature level prior to the FEB injection. Note that

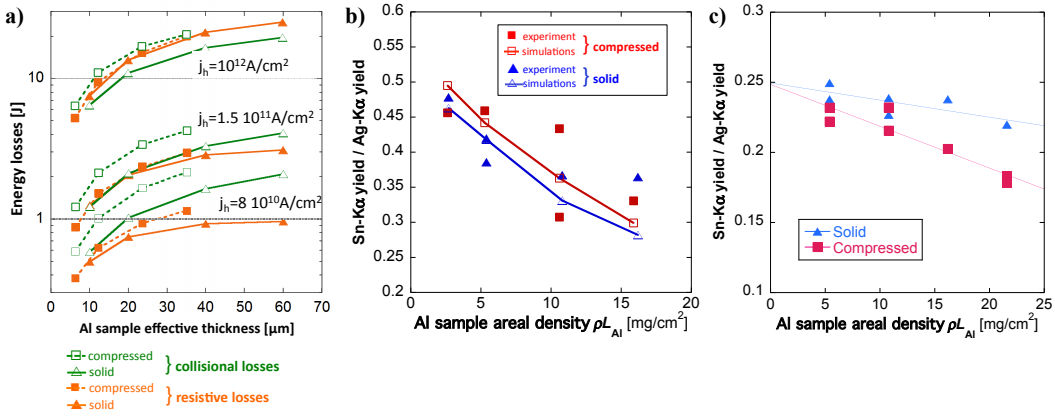

Figure 2: **a)** Calculated integrated FEB energy losses against the Al-sample effective thickness. **b)** and **c)** Target rear-side-fluorescence yield (Sn-Kα) over the front-side-fluorescence yield (Ag-Kα), against the Al-sample areal density: **b)** Experimental data (full symbols) and simulated (open symbols) from the LULI2000 experiment (35 J, 10^{19} W/cm^2), and **c)** Experimental data from the TITAN-JLF experiment (135 J, 10^{20} W/cm^2).

the resistive losses are not negligible in this regime, being only about a factor two lower than the collisional losses in both solid and compressed Al. From simulations, we can assess the hierarchy of the energy loss mechanisms for higher current densities.

For $j_h > 10^{11}$ A/cm^2, the resistive and collisional effects losses are at the same level in solid Al. The resistive losses are slightly increased in compressed matter, but only for thicknesses $> 20\,\mu$m. This prediction was confirmed experimentally using the TITAN-JLF facility. This is evidenced by the steepest drop of the fluorescence ratio Sn-K$_\alpha$/Ag-K$_\alpha$ as a function of the sample areal density found in compressed targets [Fig. 2-c)].

For $j_h > 10^{12}$ A/cm^2, the target is rapidly heated to a level where the conductivity is governed by the electron-ion collisions (Spitzer regime), independent of its initial (shock-induced) temperature. The resistive losses then hardly differ between the solid and compressed cases, which seems to rule out any clear experimental signature of resistive effects in the high-current regime.

In summary, our experimental and theoretical results suggest that resistive effects play a major role for FEB current densities $j_h > 5 \cdot 10^{11}$ A/cm^2. Though still restricted to under-scaled FI conditions, our measurements can be used for benchmarking models of FEB transport, with a predictive capability for the full-scaled, 100 kJ, 10 ps FI regime.

References

[1] M. Tabak *et al.*, Phys. Plasmas. **1**, 1626 (1994)
[2] S. Atzeni *et al.*, Phys. Plasmas. **15**, 056311 (2008)
[3] J.R. Davies *et al.*, Phys. Rev. E **56**, 7193 (1997)
[4] L. Gremillet *et al.*, Phys. Plasmas **9**, 941 (2002)
[5] J. Honrubia and J. Meyer-ter-Vehn, Nucl. Fusion, **46**, L25 (2006)
[6] E. Martinolli *et al.*, Phys. Rev. E **73**, 046402 (2006)
[7] J.J. Santos *et al.*, Phys Plasmas **14**, 103107 (2007)